Appl Phys A (2009) 95: 881–888
DOI 10.1007/s00339-009-5092-7

Applied Physics A
Materials Science & Processing

Invisibility of a metamaterial cloak illuminated by spherical electromagnetic wave

Fan-Yi Meng · Ying Liang · Qun Wu · Le-Wei Li

Received: 25 August 2008 / Accepted: 6 January 2009 / Published online: 27 January 2009

Abstract In this paper, the invisibility of a metamaterial cloak illuminated by spherical electromagnetic wave is analytically investigated based on the full wave Mie scattering model. It is shown that for a cloak with ideal parameters the scattered field intensity is zero, but for a cloak with a loss, only the backscattering is exactly zero. Moreover, in the loss case, the scattered field intensity increases as the loss increases, which is very different from that in the conventional stealth case, where the scattered field intensity decreases as the loss of coated material increases. In addition, it is shown that scattering cross-section of the cloak with perturbed parameters decreases as the thickness of the cloak decreases, which means that thinner cloak can exhibit more stable invisibility.

PACS 78.70.Gq · 81.05.Zx · 84.40.Ba

1 Introduction

In recent years, the use of abnormal refraction of metamaterial to achieve invisibility has attracted a lot of attention in the physics and engineering communities [1–10]. Different from absorbing screens and antireflection coatings to diminish the scattering or the reflection from objects, the metamaterial cloak can bend electromagnetic waves around objects, and incident wave to the cloak will render the interior effectively invisible to the outside [11–16]. To synthesize such an invisible metamaterial cloak, coordinate transformation method, which today's synthesis process of the cloak is mostly based on, and optical conformal mapping method have been proposed by Pendry et al. [1] and Leonhardt [14], respectively. Alù et al. [8, 10] have designed electrically small homogeneous metamaterial cloak based on Mie scattering theory. In analyzing the scattering characteristics of the metamaterial cloak, there are many simulation results reported on cloaking. For example, a full-wave simulation has been performed by Cummer et al. [12] to see how the material perturbation affects the invisibility. In fact, purely numerical calculations cannot provide as much insight into the physics as an analytical approach. From this point, Chen et al. [6] has established analytically the interactions of a plane wave with a spherical cloak based on Mie scattering model. However, there are still not enough analytical solutions to investigate scattering characteristics of the cloaks, especially those cloaks with perturbed material parameters under illumination of nonplanar electromagnetic wave (spherical wave, cylindrical wave, and so on).

In this paper, the scattered and transmitted fields of spherical electromagnetic wave incident onto spherical cloaks are analytically solved based on the full wave Mie scattering model. It is shown that for a cloak with ideal constitutive parameters its scattered field intensity is zero. The loss case is also investigated. Results show that the backscattering is still zero, but scattered field intensity in the other direction increases as the loss increases, which is very different from that in the conventional stealth case where the scattered field

F.-Y. Meng (✉) · Y. Liang · Q. Wu
School of Electronics and Information Technology, Harbin Institute of Technology (HIT), P.O. Box 341, Xidazhi Street, No. 92, Nangang District, Harbin, Heilongjiang 150001, P.R. China
e-mail: fymenghit@gmail.com
Fax: +86-451-86403028

L.-W. Li
Department of Electrical & Computer Engineering, National University of Singapore, Kent Ridge, Singapore 119260, Singapore
e-mail: lwli@nus.edu.sg

intensity decreases as the loss of coated material increases. In addition, the effect of constitutive parameters perturbation on scattering cross-section of the cloaks with different thickness is analyzed. It is shown that for a constant perturbation quantity, the normalized scattering cross-section of the cloak decreases as the thickness of the cloak decreases, which means that thinner cloak can bring more stable invisibility performance.

2 Exact analytical solutions for the electromagnetic model

The model configuration of interest is depicted in Fig. 1. It consists of a horizontal dipole, the spherical cloak (Region II) and the inner sphere (Region I) in free space (Region III). We assume the model in a spherical coordinates. The dipole is put at (0, 0, b) horizontally. The inner sphere has a permittivity of ε_1 and a permeability of μ_1. The spherical cloak has the thickness of $R_2 - R_1$, and is a kind of inhomogeneous anisotropic metamaterial. The constitutive parameter of the cloak has the following second order tensor form

$$\begin{aligned}\overline{\overline{\varepsilon}}(r) &= \begin{Bmatrix} \varepsilon_r & 0 & 0 \\ 0 & \varepsilon_t & 0 \\ 0 & 0 & \varepsilon_t \end{Bmatrix}, \\ \overline{\overline{\mu}}(r) &= \begin{Bmatrix} \mu_r & 0 & 0 \\ 0 & \mu_t & 0 \\ 0 & 0 & \mu_t \end{Bmatrix},\end{aligned} \tag{1}$$

where ε_r, μ_r are the permittivity and permeability in the r-direction, and ε_t, μ_t are permittivity and permeability in the θ-direction and ϕ-direction. To solve the scattering problem shown in Fig. 1, fist we should establish the wave equations in each region to get general solutions.

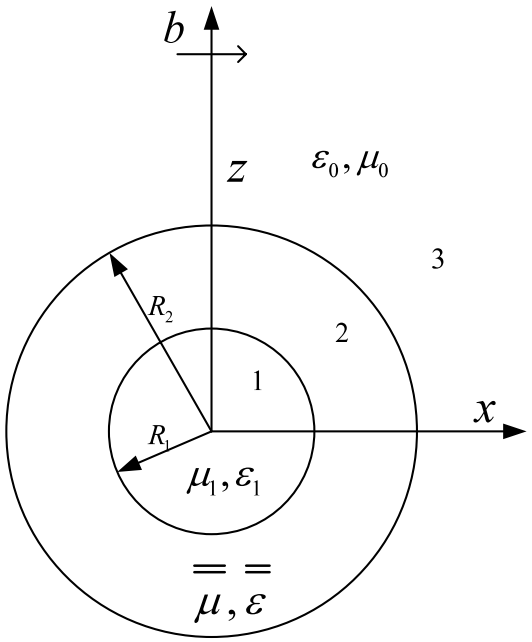

Fig. 1 Configuration of the model

To solve the problem, the general solution in each region should be solved. In the regions I ($r < R_1$) and II ($r > R_2$), where homogeneous isotropic materials are located, the wave equations and general solutions have been given by classic Mie method. But in the region III ($R_1 < r < R_2$), we must do some special manipulations because of the inhomogeneous anisotropic metamaterial.

According to Mie theory, the electromagnetic fields can be decomposed into TM and TE modes with respect to the r-direction. Moreover, TM and TE modes can be represented by vector potentials $\vec{A} = A_r\vec{e}_r$, $\vec{F} = F_r\vec{e}_r$ as follows

$$\begin{aligned}\vec{B}_{\mathrm{TM}} &= \nabla \times \vec{A}, \\ \vec{D}_{\mathrm{TE}} &= -\nabla \times \vec{F}, \\ \vec{B}_{\mathrm{TE}} &= \frac{1}{j\varpi}\nabla \times \left(\overline{\overline{\varepsilon}}^{-1}\nabla \times \vec{F},\right) \\ \vec{D}_{\mathrm{TM}} &= \frac{1}{j\varpi}\nabla \times \left(\overline{\overline{\mu}}^{-1}\nabla \times \vec{A}\right).\end{aligned} \tag{2}$$

Therefore, the electromagnetic fields can be expressed as

$$\begin{aligned}\vec{B} &= \nabla \times \vec{A} + \frac{1}{j\varpi}\nabla \times \left(\overline{\overline{\varepsilon}}^{-1}\nabla \times \vec{F}\right), \\ \vec{D} &= -\nabla \times \vec{F} + \frac{1}{j\varpi}\nabla \times \left(\overline{\overline{\mu}}^{-1}\nabla \times \vec{A}\right).\end{aligned} \tag{3}$$

At the same time, $\vec{A}$ and $\vec{F}$ must satisfy following Debye condition

$$\begin{aligned}\frac{\partial A_r}{\partial r} &= -j\varpi\varepsilon_t\mu_t\Phi_a, \\ \frac{\partial F_r}{\partial r} &= -j\varpi\varepsilon_t\mu_t\Phi_f\end{aligned} \tag{4}$$

and

$$\begin{aligned}-\nabla \cdot \Phi_a &= \vec{E} + j\varpi\vec{A}, \\ -\nabla \cdot \Phi_f &= \vec{H} + j\varpi\vec{F}.\end{aligned} \tag{5}$$

Substituting (4) into (2), wave equations in the cloak region are obtained by

$$\begin{aligned}\nabla \times \left(\overline{\overline{\mu}}^{-1}\nabla \times \vec{A}\right) - \varpi^2\overline{\overline{\varepsilon}}\vec{A} &= -j\varpi\overline{\overline{\varepsilon}}\nabla \cdot \Phi_a, \\ \nabla \times \left(\overline{\overline{\varepsilon}}^{-1}\nabla \times \vec{F}\right) - \varpi^2\overline{\overline{\mu}}\vec{F} &= -j\varpi\overline{\overline{\mu}}\nabla \cdot \Phi_f.\end{aligned} \tag{6}$$

Obviously, if $\vec{A}$ and $\vec{F}$ is solved from (6), all fields can be obtained through (3). Applying Debye condition, the wave equations for $\vec{A}$ and $\vec{F}$ are expressed as

$$\frac{\varepsilon_r}{\varepsilon_t}\frac{\partial^2 A_r}{\partial r^2} - j\varpi^2\mu_t\varepsilon_r A_r + \frac{1}{r^2\sin^2\theta}\frac{\partial^2 A_r}{\partial \phi^2}$$

$$+\frac{1}{r^2}\frac{1}{\sin\theta}\frac{\partial}{\partial\theta}\left(\sin\theta\frac{\partial A_r}{\partial\theta}\right)=0, \tag{7}$$

$$\frac{\mu_r}{\mu_t}\frac{\partial^2 F_r}{\partial r^2}-j\varpi^2\mu_r\varepsilon_t F_r+\frac{1}{r^2\sin^2\theta}\frac{\partial^2 F_r}{\partial\phi^2}+\frac{1}{r^2}\frac{1}{\sin\theta}\frac{\partial}{\partial\theta}\left(\sin\theta\frac{\partial F_r}{\partial\theta}\right)=0. \tag{8}$$

To solve the wave equation for $\vec{A}$, the variable separation method is applied. Assuming $A_r(r,\theta,\phi)=R(r)\Theta(\theta)\Phi(\phi)$, from (7) we obtain

$$\left\{\frac{\partial^2}{\partial r^2}+\left[k_t^2-\frac{\varepsilon_t}{\varepsilon_r}\frac{n(n+1)}{r^2}\right]\right\}R(r)=0,$$
$$k_t=\omega\sqrt{\varepsilon_t\mu_t}, \tag{9}$$

$$\frac{1}{\Theta(\theta)\sin\theta}\frac{d}{d\theta}\left(\sin\theta\frac{d\Theta(\theta)}{d\theta}\right)-\frac{m^2}{\sin^2\theta}=-n(n+1), \tag{10}$$

$$\frac{d^2\Phi}{d\phi}+m^2\Phi=0,\quad 0\le|m|\le n. \tag{11}$$

Equation (10) is the associated Legendre equation, its solution is the associated Legendre function $\Theta(\theta)=P_n^m(\cos\theta)$. For (11), its solution is well known as $\Phi(\phi)=A\cos(m\phi)+B\sin(m\phi)$, i.e., harmonic functions. For (9), if we assume that $\frac{\varepsilon_t}{\varepsilon_r}=\frac{r^2}{(r-R_1)^2}$, $r-R_1=r'$ and $R(r)=R'(r')$, then (9) can be changed into

$$\left\{\frac{\partial^2}{\partial(r')^2}+\left[k_t^2-\frac{n(n+1)}{(r')^2}\right]\right\}R'(r')=0. \tag{12}$$

Its solution is $R'(r')=k_t r' b_n(k_t r')$, so $R(r)=k_t(r-R_1)\times b_n(k_t(r-R_1))$. Here, $b_n(z)$ is the Spherical Bessel function, including the Spherical Bessel function of the first kind, $j_n(z)$, the Spherical Neumann function, $n_n(z)$, and the Spherical Hankel function of the first kind, $h_n^{(1)}(z)$, and the second Spherical Hankel function, $h_n^{(2)}(z)$. The functions $j_n(z)$ and $n_n(z)$ represent the stationary wave, while $h_n^{(1)}(z)$ and $h_n^{(2)}(z)$ represent the traveling waves. Therefore, the solution of (7) is

$$A_r^c=\sum_{m=0}^{\infty}\sum_{n=m}^{\infty}k_t(r-R_1)b_n\big(k_t(r-R_1)\big)P_n^m(\cos\theta)\times[A_{2,nm}\cos m\phi+B_{2,nm}\sin m\phi], \tag{13}$$

where $A_{2,nm}$ and $B_{2,nm}$ are the expansion coefficients. According to the principle of duality, when $\frac{\mu_t}{\mu_r}=\frac{r^2}{(r-R_1)^2}$, the general solution of $\vec{F}$ in cloak is:

$$F_r^c=\sum_{m=0}^{\infty}\sum_{n=m}^{\infty}k_t(r-R_1)b_n\big(k_t(r-R_1)\big)P_n^m(\cos\theta)\times\left[A'_{2,nm}\cos m\phi+B'_{2,nm}\sin m\phi\right], \tag{14}$$

where $A'_{2,nm}$ and $B'_{2,nm}$ are the expansion coefficients. In this case, the general solution of electric fields and magnetic field can be obtained by substituting (13) and (14) into (3).

In the dielectric sphere and the free space regions, the general solutions of vector potentials can be easily obtained by a similar argument as in (2)–(14). In the dielectric sphere,

$$\begin{aligned}A_r^{\text{int}}&=\sum_{m=0}^{\infty}\sum_{n=m}^{\infty}k_1 r b_n(k_1 r)P_n^m(\cos\theta)\times[A_{1,nm}\cos m\phi+B_{1,nm}\sin m\phi],\\ F_r^{\text{int}}&=\sum_{m=0}^{\infty}\sum_{n=m}^{\infty}k_1 r b_n(k_1 r)P_n^m(\cos\theta)\times\left[A'_{1,nm}\cos m\phi+B'_{1,nm}\sin m\phi\right],\end{aligned} \tag{15}$$

where $k_1=\omega\sqrt{\varepsilon_1\mu_1}$ is the propagation constant in the dielectric sphere, $A_{1,nm}$, $B_{1,nm}$, $A'_{1,nm}$, $B'_{1,nm}$ are expansion coefficients. And in free space,

$$\begin{aligned}A_r^s&=\sum_{m=0}^{\infty}\sum_{n=m}^{\infty}k_0 r b_n(k_0 r)P_n^m(\cos\theta)\times[A_{3,nm}\cos m\phi+B_{3,nm}\sin m\phi],\\ F_r^s&=\sum_{m=0}^{\infty}\sum_{n=m}^{\infty}k_0 r b_n(k_0 r)P_n^m(\cos\theta)\times\left[A'_{3,nm}\cos m\phi+B'_{3,nm}\sin m\phi\right],\end{aligned} \tag{16}$$

where $k_0=\omega\sqrt{\varepsilon_0\mu_0}$ is the propagation constant in free space, $A_{3,nm}$, $B_{3,nm}$, $A'_{3,nm}$, $B'_{3,nm}$ are expansion coefficients.

At the same time, the exact expression of incident wave radiated by the horizontal electric dipole is needed. The radiated wave of the dipole can be calculated by the Green function method as

$$\vec{E}^i(r)=-j\varpi\mu\int_V\overline{\overline{G_0}}(\vec{r}|\vec{r}')\cdot\vec{J}(\vec{r}')\,dV', \tag{17}$$

where

$$\vec{J}(\vec{r}')=Il\frac{\delta(r'-b)\delta(\theta'-0)\delta(\phi'-0)}{b^2\sin\theta'}\vec{u}_x. \tag{18}$$

In (18), $\vec{u}_x$ is the unit vector in the x-direction, it can be rewritten in the spherical coordinates as $\vec{u}_x=\sin\theta\cos\phi\vec{\mu}_r+\cos\theta\cos\phi\vec{\mu}_\theta+\sin\phi\vec{\mu}_\phi$. By some algebraic manipulations with (17), the Ampere's Law of Maxwell equation and the following relationship derived from Debye condition

$$\begin{aligned}A_r&=\frac{j\varpi\varepsilon_0\mu_0 r^2}{n(n+1)}E_r,\\ F_r&=\frac{j\varpi\varepsilon_0\mu_0 r^2}{n(n+1)}H_r,\end{aligned} \tag{19}$$

vector potentials of the horizontal dipole can be calculated as

$$
\begin{aligned}
A_r^i &= \cos\phi \sum_n a_n k_0 r j_n(k_0 r) P_n^1(\cos\theta),\\
F_r^i &= \sin\phi \sum_n b_n k_0 r j_n(k_0 r)\\
&\quad \times \big\{\big[n+3+(n+1)\cos(2\theta)P_n^1(\cos\theta)\big]\\
&\quad + 2\big[(-2n-3)\cos\theta P_{n+1}^1(\cos\theta)\big]\\
&\quad + (n+1)P_{n+2}^1(\cos\theta)\big\}
\end{aligned}
\tag{20}
$$

where

$$
\begin{aligned}
a_n &= j\frac{(2n+1)\mu_0}{8n(n+1)bk_0\pi} h_n^{(2)'}(k_0 b),\\
b_n &= \frac{(2n+1)\varpi k_0 \varepsilon_0 \mu_0}{16\pi n(n+1)^2} h_n^{(2)}(k_0 b)\cos^2\theta.
\end{aligned}
\tag{21}
$$

At $r = R_1$ and $r = R_2$, the boundary conditions are given by

$$
\begin{aligned}
&\frac{A_r^{in}(R_1)}{\mu_1} = \frac{A_r^c(R_1)}{\mu_t}, \qquad \frac{A_r^i(R_2)+A_r^s(R_2)}{\mu_0} = \frac{A_r^c(R_2)}{\mu_t},\\
&\frac{F_r^{in}(R_1)}{\varepsilon_1} = \frac{F_r^c(R_1)}{\varepsilon_t}, \qquad \frac{F_r^i(R_2)+F_r^s(R_2)}{\varepsilon_0} = \frac{F_r^c(R_2)}{\varepsilon_t},\\
&\frac{A_r^{in'}(R_1)}{\varepsilon_1\mu_1} = \frac{A_r^{c'}(R_1)}{\varepsilon_t\mu_t}, \qquad \frac{A_r^{i'}(R_2)+A_r^{s'}(R_2)}{\varepsilon_0\mu_0} = \frac{A_r^{c'}(R_2)}{\varepsilon_t\mu_t},\\
&\frac{F_r^{in'}(R_1)}{\varepsilon_1\mu_1} = \frac{F_r^{c'}(R_1)}{\varepsilon_t\mu_t}, \qquad \frac{F_r^{i'}(R_2)+F_r^{s'}(R_2)}{\varepsilon_0\mu_0} = \frac{F_r^{c'}(R_2)}{\varepsilon_t\mu_t}.
\end{aligned}
\tag{22}
$$

Substituting (13), (14), (15), (16), and (20) into (22), the vector potentials of scattered and transmitted fields are obtained as

$$
\begin{aligned}
A_r^s &= \cos\phi \sum_n A_{3,n} k_0 r h_n^{(2)}(k_0 r) P_n^1(\cos\theta),\\
F_r^s &= \sin\phi \sum_n B'_{3,n} k_0 r h_n^{(2)}(k_0 r)\\
&\quad \times \big\{\big[n+3+(n+1)\cos(2\theta)P_n^1(\cos\theta)\big]\\
&\quad + 2\big[(-2n-3)\cos\theta P_{n+1}^1(\cos\theta)\big]\\
&\quad \times + (n+1)P_{n+2}^1(\cos\theta)\big\},\\
A_r^c &= \cos\phi \sum_n A_{2,n} k_t (r-R_1) j_n\big(k_t(r-R_1)\big) P_n^1(\cos\theta),\\
F_r^c &= \sin\phi \sum_n B'_{2,n} k_t (r-R_1) j_n\big(k_t(r-R_1)\big)\\
&\quad \times \big\{\big[n+3+(n+1)\cos(2\theta)P_n^1(\cos\theta)\big]\\
&\quad + 2\big[(-2n-3)\cos\theta P_{n+1}^1(\cos\theta)\big]\\
&\quad +(n+1)P_{n+2}^1(\cos\theta)\big\},\\
A_r^{in} &= \cos\phi \sum_n A_{1,n} k_1 r j_n(k_1 r) P_n^1(\cos\theta),\\
F_r^{in} &= \sin\phi \sum_n B'_{1,n} k_1 r j_n(k_1 r)\\
&\quad \times \big\{\big[n+3+(n+1)\cos(2\theta)P_n^1(\cos\theta)\big]\\
&\quad + 2\big[(-2n-3)\cos\theta P_{n+1}^1(\cos\theta)\big]\\
&\quad +(n+1)P_{n+2}^1(\cos\theta)\big\},
\end{aligned}
\tag{23--25}
$$

where

$$
\begin{aligned}
A_{1,n} &= \frac{\mu_t}{\mu_0} a_n,\\
B'_{1,n} &= \frac{\varepsilon_t}{\varepsilon_0} b_n,\\
A_{2,n} &= \frac{-j_n(k_t(R_2-R_1))j_n'(k_0R_2) + (\varepsilon_t/\varepsilon_0) j_n(k_0R_2) j_n'(k_t(R_2-R_1))}{j_n(k_t(R_2-R_1))h_n^{(2)'}(k_0R_2) + (\varepsilon_t/\varepsilon_0) j_n(k_0R_2) h_n^{(2)'}(k_t(R_2-R_1))} a_n,\\
B'_{2,n} &= \frac{-j_n(k_t(R_2-R_1))j_n'(k_0R_2) + (\mu_t/\mu_0) j_n(k_0R_2) j_n'(k_t(R_2-R_1))}{j_n(k_t(R_2-R_1))h_n^{(2)'}(k_0R_2) + (\mu_t/\mu_0) j_n(k_0R_2) h_n^{(2)'}(k_t(R_2-R_1))} b_n,\\
A_{1,n} &= 0,\\
B'_{1,n} &= 0.
\end{aligned}
\tag{26}
$$

If substituting

$$
\varepsilon_t = \varepsilon_0 \frac{R_2}{R_2-R_1}, \qquad \varepsilon_r = \varepsilon_t \frac{(r-R_1)^2}{r^2}
$$

and

$$
\mu_t = \mu_0 \frac{R_2}{R_2-R_1}, \qquad \mu_r = \mu_t \frac{(r-R_1)^2}{r^2}
$$

into (26), one can obtain that $A_{2,n} = 0$ and $B'_{2,n} = 0$. It means that the scattered field intensity of the cloak is exactly zero.

3 Calculation results

Although (26) shows that the scattering factors are zero, we are interested in observing how the wave propagates in or-

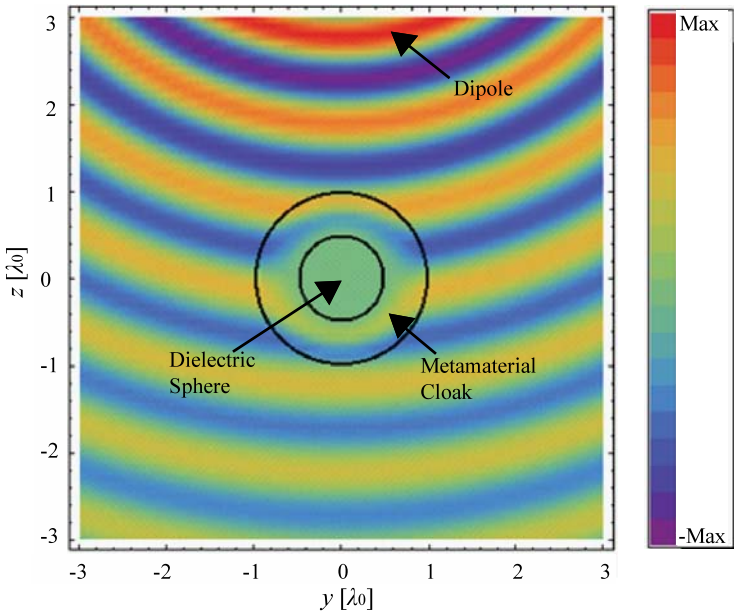

Fig. 2 Electric fields distribution (H-plane) near the cloak with $R_1 = 0.5\lambda_0$, $R_2 = \lambda_0$

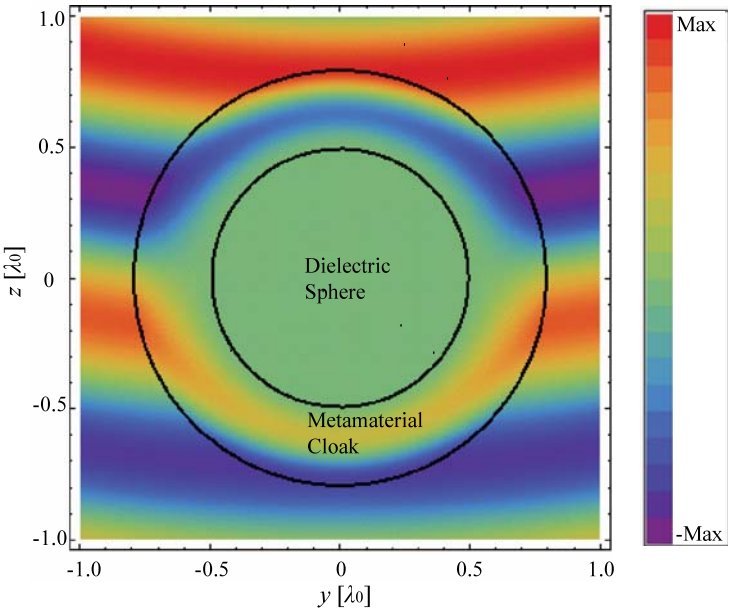

Fig. 3 Electric field distribution (H-plane) near the cloak when $R_1 = 0.5\lambda_0$, $R_2 = 0.8\lambda_0$

der to understand the invisibility principle. Figure 2 shows the calculated electric fields due to an spherical wave incidence onto a cloak with $R_1 = 0.5\lambda_0$ and $R_2 = \lambda_0(\lambda_0$ denotes the wavelength in free space). From Fig. 2, it can be seen that the wave is guided around the spherical object as if nothing were there after the wave comes into the cloak without any reflection. Therefore, in this case, there are two important points to realize invisibility. The first is the impedance match between the cloak and the free space, which makes the wave come in and come out freely between the cloak and the free space without any reflection. The second is the specific refraction characteristics of electromagnetic waves in the cloak, which makes the wave propagate on a specific track. Figure 3 shows the electric field distribution near the cloak when $R_1 = 0.5\lambda_0$ and $R_2 = 0.8\lambda_0$. Figure 4 shows the electric field distribution when $R_1 = 0.5\lambda_0$ and $R_2 = 0.6\lambda_0$. Comparing Fig. 3 with Fig. 4, it can be seen that the refraction angle at the interface between the cloak and free space increases as the cloak thins, while the hidden object keeps completely hidden from waves.

The most interesting thing is that (26) gives further information. For example, the loss is often an important issue. When the electric and magnetic loss tangents are introduced, the scattering coefficients become nonzero. Define the normalized far field (NFF) as $NFF = 20\log|\frac{\bar{W}^s+\bar{W}^i}{\bar{W}^i}| =$

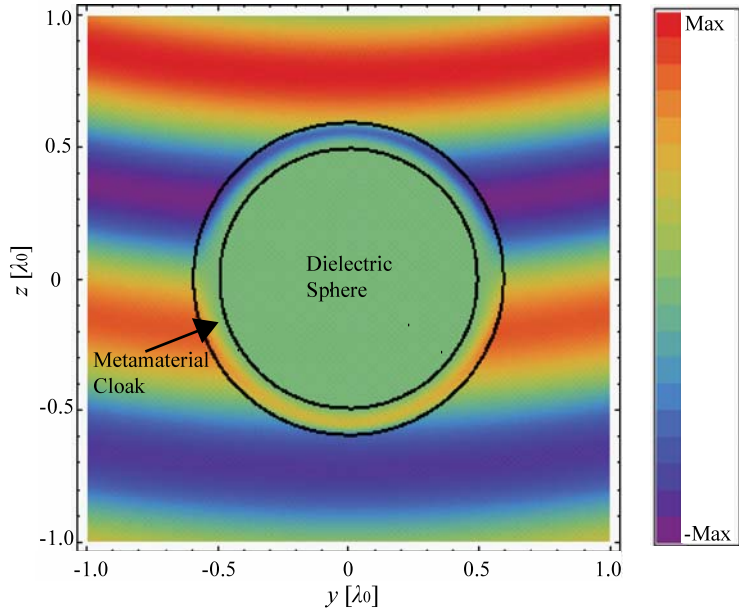

Fig. 4 Electric field distribution (H-plane) near the cloak when $R_1 = 0.5\lambda_0$, $R_2 = 0.6\lambda_0$

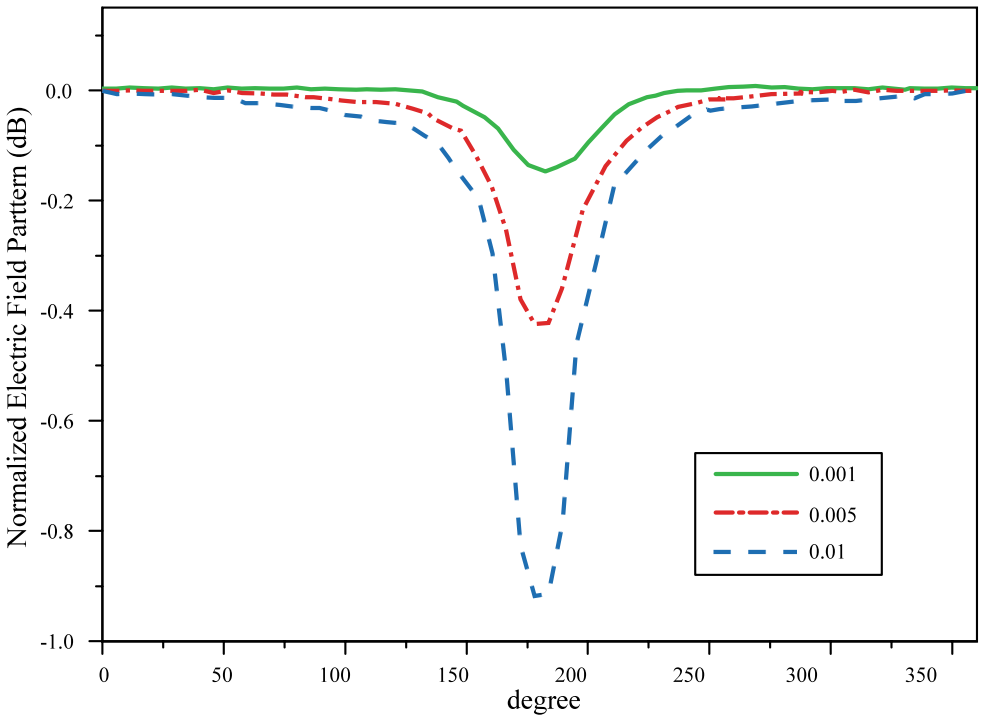

Fig. 5 Normalized electrical far field (H-plane) with cloak of for different loss tangent

$20\log|1+\frac{\bar{W}^s}{\bar{W}^i}|$, where $\bar{W}^s$ is the scattered electric field $\bar{E}^s$ or the magnetic field $\bar{H}^s$, and $\bar{W}^i$ is the incident electric $\bar{E}^i$ or the magnetic field $\bar{H}^i$. Figure 5 shows the normalized far field pattern (electric field in H-plane) of cloaks with loss tangent of 0.001, 0.005. From Fig. 5, it can be seen that the backscattering ($\theta = 0^o$) is still zero, but scattered field intensity in the other direction increases as the loss increases, which is very different from that in the conventional stealth case, where the scattered field intensity decreases as the loss of coated material increases.

Since it is known that the constitutive parameters for a perfect cloak are very difficult to realize, non-ideal material parameters are more often used in the measurements. Hence, it is necessary to study how the constitutive parameters' perturbation quantitatively affects the performance of the cloak. Figure 6 shows the calculated normalized radar cross-section $Q_{\text{sca}} = \frac{2}{(k_0 R_2)^2}\sum_n (2n+1)(|A_{2,n}|^2 + |B'_{2,n}|^2)$ as a function of the normalized permittivity $\varepsilon_t(R_2 - R_1)/\varepsilon_0 R_2$ for $R_2 - R_1 = 0.1\lambda_0, 0.3\lambda_0$, and $0.5\lambda_0$ when

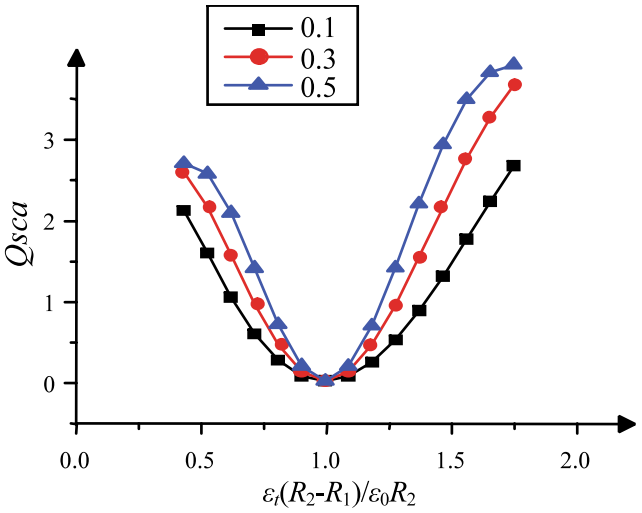

Fig. 6 Normalized scattering cross section of cloaks of different thickness $R_2 - R_1$ as a function of $\varepsilon_t(R_2 - R_1)/\varepsilon_0 R_2$ for $R_2 - R_1 = 0.1\lambda_0$, $0.3\lambda_0$, and $0.5\lambda_0$ when $\mu_t = \mu_0 R_2/(R_2 - R_1)$ and $R_1 = 0.5\lambda_0$

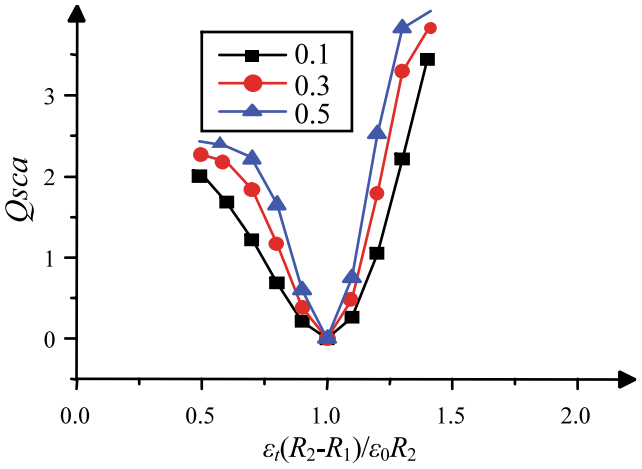

Fig. 7 Normalized scattering cross section of cloaks of different thickness $R_2 - R_1$ as a function of $\varepsilon_t(R_2 - R_1)/\varepsilon_0 R_2$ for $R_2 - R_1 = 0.1\lambda_0$, $0.3\lambda_0$, and $0.5\lambda_0$ when $\mu_t = \eta_0^2 \varepsilon_t$ and $R_1 = 0.5\lambda_0$

$\mu_t = \mu_0 R_2/(R_2 - R_1)$ and $R_1 = 0.5\lambda_0$. From Fig. 6, it can be seen that Q_{sca} increases as ε_t changes from the ideal parameter. Moreover, for a constant perturbation quantity, Q_{sca} decreases as $R_2 - R_1$ decreases, which means that a thinner cloak can bring more stable invisibility characteristics. Figure 7 shows the Q_{sca} as a function of $\varepsilon_t(R_2 - R_1)/\varepsilon_0 R_2$ for $R_2 - R_1 = 0.1\lambda_0, 0.3\lambda_0$, and $0.5\lambda_0$ when $\mu_t = \eta_0^2 \varepsilon_t$ and $R_1 = 0.5\lambda_0$. In this case, the characteristic impedance of the cloak is constant. From Fig. 7, it can be seen that Q_{sca} increases more rapidly than that shown in Fig. 6. The reason is that μ_t in the case of Fig. 7 changes in direction ratio with ε_t, which leads to a more rapid change in the refractive index than that in the case of Fig. 6, where μ_t is constant. It can be also seen from Fig. 7 that Q_{sca} decreases as $R_2 - R_1$ decreases, which is in good agreement with that shown in Fig. 6.

4 Conclusions

A metamaterial cloak illuminated by spherical electromagnetic wave is rigorously analyzed. It is demonstrated that metamaterial cloak with ideal parameters can be absolutely invisible to a spherical incident wave. The field distribution near the cloak is calculated and plotted. It is shown that metamaterial cloak bends the electromagnetic wave around the inner sphere. The scattering characteristics of the imperfect cloak with loss and perturbed parameters are also analytically established. The normalized far field patterns of the cloak with different loss are calculated and compared. It is shown that the scattered field intensity increases as the loss increases. The normalized radar cross-section of the cloak with perturbed parameters of different thickness are calculated and compared. It is shown that scattering cross-section of the cloak decreases as the cloak thins, which means that a thinner cloak can exhibit more stable invisibility.

Acknowledgements This work is supported by the National Natural Science Foundation of China (Nos. 60801015, 60571026), Development Program for Outstanding Young Teachers in Harbin Institute of Technology (No. HITQNJS.2008.007), China Postdoctoral Science Foundation funded project (No. 20070420158), Heilongjiang Postdoctorial Financial Assistance (No. LBH-Z07083), and Ph.D. programs foundation of the ministry of education of China (No. 200802131075).

References

1. J.B. Pendry, D. Schurig, D.R. Smith, Controlling electromagnetic fields. Science **312**, 1780–1782 (2006)
2. H. Chen, C.T. Chan, Acoustic cloaking in three dimensions using acoustic metamaterials. Appl. Phys. Lett. **91**, 183518 (2007)
3. A. Greenleaf, Y. Kurylev, M. Lassas, G. Uhlmann, Improvement of cylindrical cloaking with the SHS lining. Opt. Express **15**, 12717–12734 (2007)
4. O. Ozgun, M. Kuzuoglu, Electromagnetic metamorphosis: Reshaping scatterers via conformal anisotropic metamaterial coatings. Microw. Opt. Technol. Lett. **49**, 2386–2392 (2007)
5. Y. Huang, Y. Feng, T. Jiang, Electromagnetic cloaking by layered structure of homogeneous isotropic materials. Opt. Express **15**, 11133–11141 (2007)
6. H. Chen, B.-I. Wu, B. Zhang, J.A. Kong, Electromagnetic wave interactions with a metamaterial cloak. Phys. Rev. Lett. **99**, 063903 (2007)
7. F.L. Teixeira, Differential form approach to the analysis of electromagnetic cloaking and masking. Microw. Opt. Technol. Lett. **49**, 2051–2053 (2007)
8. A. Alu, N. Engheta, Cloaking and transparency for collections of particles with metamaterial and plasmonic covers. Opt. Express **15**, 7578–7590 (2007)
9. A. Hakansson, Cloaking of objects from electromagnetic fields by inverse design of scattering optical elements. Opt. Express **15**, 4328–4334 (2007)
10. A. Alu, N. Engheta, Plasmonic materials in transparency and cloaking problems: mechanism, robustness, and physical insights. Opt. Express **15**, 3318–3332 (2007)

11. M.G. Silveirinha, A. Alu, N. Engheta, Parallel-plate metamaterials for cloaking structures. Phys. Rev. E, Stat. Nonlinear Soft Matter Phys. **75**, 036603 (2007)
12. S.A. Cummer, B.-I. Popa, D. Schurig, D.R. Smith, Full-wave simulations of electromagnetic cloaking structures. Phys. Rev. E **74**, 036621 (2006)
13. D. Schurig, J.J. Mock, B.J. Justice, S.A. Cummer, J.B. Pendry, A.F. Starr, D.R. Smith, Metamaterial electromagnetic cloak at microwave frequencies. Science **314**, 977–980 (2006)
14. U. Leonhardt, Optical conformal mapping. Science **312**, 1777–1780 (2006)
15. U. Leonhardt, Notes on conformal invisibility devices. New J. Phys. **8**, 118 (2006)
16. A. Hendi, J. Henn, U. Leonhardt, Ambiguities in the scattering tomography for central potentials. Phys. Rev. Lett. **97**, 073902 (2006)